Journal of Molecular Structure 1278 (2023) 134920

Contents lists available at ScienceDirect

Journal of Molecular Structure

journal homepage: www.elsevier.com/locate/molstr

New imidazole derivatives as aromatase inhibitor: Design, synthesis, biological activity, molecular docking, and computational ADME-Tox studies

Gökay Çetiner[a], Ulviye Acar Çevik[a,*], Ismail Celik[b], Hayrani Eren Bostancı[c], Yusuf Özkay[a], Zafer Asım Kaplancıklı[a]

[a] Department of Pharmaceutical Chemistry, Faculty of Pharmacy, Anadolu University, Eskişehir 26470, Turkey
[b] Department of Pharmaceutical Chemistry, Faculty of Pharmacy, Erciyes University, Kayseri 38039, Turkey
[c] Department of Biochemistry, Faculty of Pharmacy, Sivas Cumhuriyet University, Sivas, Turkey

ARTICLE INFO

Article history:
Received 2 November 2022
Revised 20 December 2022
Accepted 4 January 2023
Available online 6 January 2023

Keywords:
Synthesis
Imidazole
Anticancer activity
Aromatase
Docking ADME-Tox

ABSTRACT

In this study, a series of imidazole derivatives was designed, synthesized, and evaluated for *in vitro* biological activity on the human breast cancer cell line MCF7 by MTT assay. To determine the selectivity of the compounds, their cytotoxic effects on the L929 (healthy mouse fibroblast) cell line were also investigated. Compounds **1a, 1b**, and **1d** were found to be more effective than the reference drug cisplatin against the MCF7 cell line. It is seen that the cytotoxic effects of the compounds on the L929 cell line are quite low, and the compounds are found to be highly selective. The inhibition potentials of the compounds **1a, 1b, 1d**, and **1k** which were effective on the MCF7 cell line, and on the aromatase enzyme were evaluated and it was found that the compounds had similar effects to the reference drug letrozole. Further, the interactions between the best active compounds and the human aromatase cytochrome P450 (CYP) enzyme were analyzed through a molecular docking study. The findings suggest that these compounds could be a promising candidate for the creation of a new family of non-steroidal aromatase inhibitors. Finally, computational ADME-Tox studies of compounds **1a, 1b, 1d**, and **1k** were performed and found to have the appropriate profile.

1. Introduction

Breast cancer is the most common cancer among women, affecting almost 2.1 million people each year and being the leading cause of cancer-related deaths [1]. Breast cancer risk is higher in postmenopausal women due to estrogen production in peripheral tissues. Estrogen has an important function in encouraging neoplastic breast epithelial cell development in breast cancer patients with positive estrogen receptors via signaling estrogen receptor-mediated pathways. As a result, elevated estrogen levels have been linked to an increased risk of recurrence and metastasis in hormone-dependent breast cancer patients [2,3].

Estrogen production is carried out by the aromatase cytochrome P450 (CYP) enzyme complex. The Cytochromes P450 (CYP450) enzymes are responsible for catalyzing the aromatization of these compounds' six-membered alicyclic moiety to generate estrogen rings [2,4]. Through three hydroxylation reaction steps, CYP19 transforms C19 androgens (androstenedione and testosterone) into aromatic C18 estrogens (estradiol and estrone). High estrogen levels have been linked to the development of hormone-dependent breast cancer (HDBC) and metastases in both premenopausal and postmenopausal women [5,6]. Aromatase inhibitors (AI) have the potential to block or inactivate the aromatase enzyme, preventing estrogen production and consequently cell proliferation [7–10].

Several aromatase inhibitors, categorized as steroidal and non-steroidal (Fig. 1), working via a competitive or non-competitive mechanism of action, have been identified as a result of decades of research [11,12]. New non-steroidal aromatase inhibitors with improved selectivity and potency, as well as fewer and milder adverse effects, are being developed by researchers. Nonsteroidal aromatase inhibitors have two primary elements in their structure. The azole part containing a nitrogen atom interacts with the heme-iron atom of aromatase cytochrome P450, while the bulky aryl part resembles the substrate's steroid ring [13,14].

In this study, new imidazole derivative compounds similar in structure to letrozole were designed. We planned to search for more effective anti-aromatase molecular new entities and adopted a scaffold hopping strategy. Scaffold-hopping has been a popular

* Corresponding author.
E-mail address: uacar@anadolu.edu.tr (U. Acar Çevik).

https://doi.org/10.1016/j.molstruc.2023.134920
0022-2860/

approach to discovering structurally novel potent compounds with improved properties [15,16]. The imidazole ring is used instead of the triazole structure, and an extra heteroaromatic group is added to the imidazole ring (Fig. 1). In addition, molecular docking studies are a method used in drug designs to predict how new compounds interact or do not interact with macromolecules. The interaction of the designed compounds with CYP450 was examined by molecular docking. Binding poses and docking interaction energies suggested that there may be interaction with key amino acids at the CYP450 active site like letrozole.

MTT assay was used to assess cell viability and cytotoxicity of all final compounds on MCF7 breast cancer cells. In a fluorimetric *in vitro* assay, the most active compounds were tested against aromatase and compared to letrozole. The most promising compounds were further subjected to docking tests to determine their binding mechanism in the human aromatase active site, and *in silico* absorption, distribution, metabolism, excretion (ADME), and toxicity (ADME-Tox) profile studies were performed.

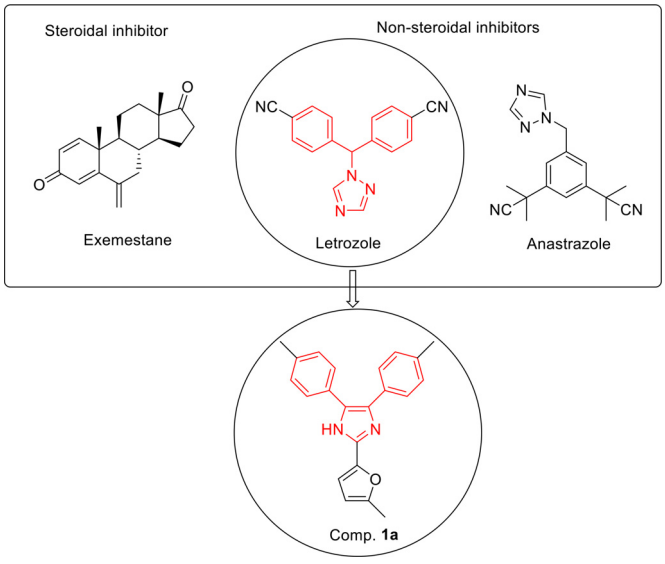

Fig. 1. Chemical structures of third-generation aromatase inhibitors exemestane, letrozole, anastrozole, and design strategy of compound **1a**.

2. Result and discussion

2.1. Chemistry

The multicomponent reactions (MCR) have favorable attributes, especially atom economy, as well as efficient generation of chemical diversity [17,18]. The target molecules were synthesized one step as depicted in Scheme 1.

The Debus–Radziszewskire action allows the straight forward synthesis of imidazoles from 1,2-diketones, aldehydes and a source of ammonia such as ammonium acetate. Imidazole ring construction was accomplished with the one-pot synthesis, which allowed time-saving. Benzyl derivative, aldehyde derivative, and ammonium acetate in acetic acid were refluxed for 3 h while stirring to obtain the final compounds [19,20]. The synthesis mechanism of the compounds is given in Fig. 2. The reaction can be viewed as occurring in two stages. In the first stage, the dicarbonyl and ammonia condense to give a diimine. In the second step, this diimine condenses with the aldehyde to give the imidazole ring.

The chemical structures of the compounds were elucidated via ^{1}H NMR, ^{13}C NMR and HRMS spectroscopic methods. Compounds **1a, 1b, 1c,** and **1d** have the p-tolyl structure in common. The -CH_3 protons in this structure were seen as singlet be-

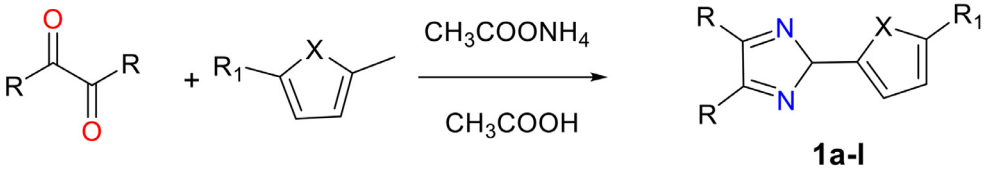

Comp.	X	R	R_1
1a	-O	4-Methylphenyl	-CH_3
1b	-O	4-Methylphenyl	-NO_2
1c	-S	4-Methylphenyl	-CH_3
1d	-NCH_3	4-Methylphenyl	-H
1e	-O	4-Fluorophenyl	-CH_3
1f	-O	4-Fluorophenyl	-NO_2
1g	-S	4-Fluorophenyl	-CH_3
1h	- NCH_3	4-Fluorophenyl	-H
1i	-O	Furan-2-yl	-CH_3
1j	-O	Furan-2-yl	-NO_2
1k	-S	Furan-2-yl	-CH_3
1l	- NCH_3	Furan-2-yl	-H

Scheme 1. Chemical structure and general procedure for the synthesis of the final compounds **1a-1l**

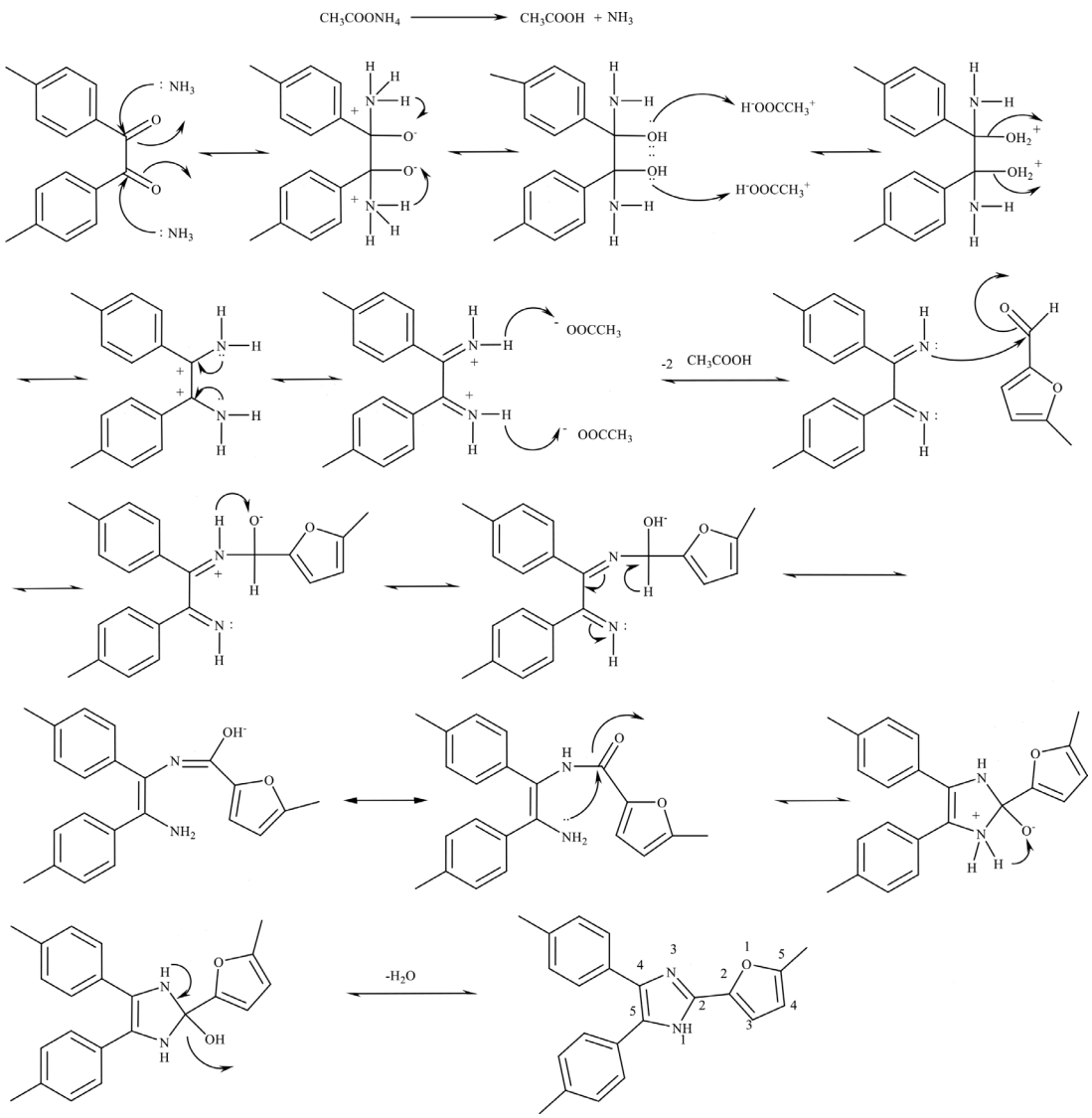

Fig. 2. Synthesis mechanism of compound **1a**.

tween 2.30–2.41 ppm. CH_3 protons in the 5th position of the furan ring in compounds **1a, 1e**, and **1i** were seen as singlet between 2.34–2.38 ppm. CH_3 protons in the 5th position of the thiophene ring in compounds **1c**, 1 g, and **1k** were seen as singlet between 2.34–2.50 ppm. CH_3 protons in 1-methylpyrrole structure in compounds **1d**, 1 h, and **1l** were recorded as singlet between 3.37–3.88 ppm. The aromatic protons of the furan, thiophen and pyrrol rings were observed in the range of 6.23–8.25, 7.67–8.18 and 6.22–6.99 ppm, respectively. The peaks of the protons on the 1,4-disubstitutedphenyl ring were observed as two doublets in the range of 7.13–8.06 ppm. In the synthesized compounds, the common structural particles gave peaks in the ^{13}C NMR spectra as expected in general. Methyl protons in the structures of the compounds were observed in the range of 13.86–36.92 ppm. In the spectra of the synthesized compounds, the total carbon number was determined by considering the identical carbon atoms according to their electronic environment, and the expected number of peaks was observed. The HRMS analysis confirmed the mass with the calculated values of the target compounds.

Table 1
IC_{50} values (μM) of compounds **1a-1l** and reference drug cisplatin for MCF-7 and L929 cell lines.

Comp.	MCF-7	L929
1a	7.9 μM±0.218	>100mM
1b	8.2 μM±0.309	>100mM
1c	>100mM	>100mM
1d	8.7 μM±0.318	>100mM
1e	>100mM	>100mM
1f	>100mM	>100mM
1 g	>100mM	>100mM
1h	>100mM	>100mM
1i	>100mM	>100mM
1j	>100mM	87.8 μM±3.780
1k	10.09 μM±0.402	>100mM
1l	>100mM	>100mM
Cisplatin	9.75 μM±0.374	>100mM
Letrozole	4.70±0.204	>100mM

2.2. Cytotoxicity assay

The anticancer activity results of compounds **1a-1l** against MCF7 and L929 are presented in Table 1. In addition, the% cell inhibition plot of compounds **1a, 1b, 1d, 1k** and cisplatin *versus* administered drug concentrations is shown in Fig. 3. When the cytotoxic effects of the synthesized compounds on the MCF7 cell line were evaluated, it was determined that the compounds **1a, 1b, 1d**, and **1k** had promising effects in the series. In particular, it was determined that the IC_{50} value (7.9 μM) of compound **1a** was higher

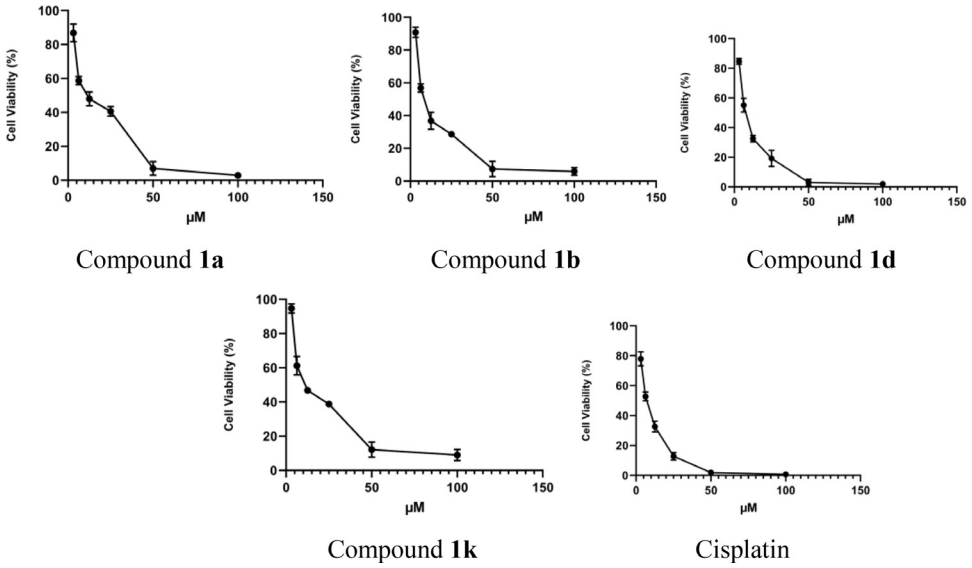

Fig. 3. % Cell inhibition graph of compounds **1a, 1b, 1d, 1k** and cisplatin against administered drug concentrations.

than cisplatin (9.75 μM). In addition, compounds **1b** and **1d** were found to have higher efficacy than cisplatin, with IC_{50} values of 8.2 μM and 8.7 μM, respectively. Three different diketone derivatives, 4,4′-dimethylbenzyl, α-furyl and 4,4′-difluorobenzyl, were used in the synthesis of the compounds. It was seen that especially 4,4′-dimethylbenzyl derivative compounds come to the forefront in terms of activity. In particular, compound **1a** containing the 5-methylfuran ring in the 2nd position of the imidazole ring has the highest activity in the series. It is seen that the compound **1b** carrying the 5-nitrofuran ring exhibits activity close to the compound **1a**. The presence of a methyl or nitro group in the 5th position of the furan ring did not cause a significant change in activity. Among the compounds with 1-methyl-1*H*-pyrrol structure (**1d**, 1 h and **1l**), it is seen that compound **1d** with 4-methylphenyl structure exhibits the highest activity. Among the compounds bearing furan ring at the 4th and 5th positions of the imidazole ring (**1i, 1j, 1k** and **1l**), compound **1k** with 5-methylthiophene structure was found to have the highest activity. The L929 healthy mouse fibroblast cell line was used to determine the selectivity of the compounds. The cytotoxic effect of the synthesized compounds on the healthy cell line was found similar to the reference drug cisplatin and is promising. Compounds **1a, 1b, 1d**, and **1k**, which were found to be effective on the MCF-7 cancer cell line, were selected for *in vitro* aromatase activity.

2.3. Aromatase inhibition assay

The aromatase enzyme is a member of the cytochrome P450 enzyme that catalyzes the biosynthesis of androgen to estrogen. Estrogen levels have been found to be high in breast cancers. Therefore, the use of aromatase inhibitors in estrogen-dependent breast cancers is one of the current therapeutic strategies [21]. Therefore, the aromatase inhibition potentials of derivatives (**1a, 1b, 1d**, and **1k**) active against the MCF-7 cancer cell line were evaluated.

The *in vitro* anti-aromatase activity of the most active compounds **1a, 1b, 1d**, and **1k** was evaluated using the commercial fluorimetric assay kit (Aromatase-CYP19A Inhibitor Screening kit, BioVIsion) with letrozole as the reference drug. The results are presented in Table 2. It was determined that the compounds have IC_{50} value ranges of 5.418–8.786 μM. These values indicated that the compounds have a lower effect than letrozole. Among the compounds, compound **1a** one was found to have the highest activity with an IC_{50} value of 5.418±0.170 μM.

Table 2
IC_{50} (μM) values of compounds.

Compounds	Aromatase Inhibition (IC_{50})
1a	5.418±0.170
1b	8.786±0.195
1d	6.805±0.119
1k	6.138±0.210
Letrozole	0.114±0.003

2.4. Molecular docking analysis

Molecular docking studies are used to predict protein-ligand interactions at the atomic level [22–24]. Molecular docking analyses are also used in structure-based drug designs to calculate the interaction energies of small molecule compounds with macromolecules [25]. In this study, molecular docking studies of 2,4,5-trisubstituted diazole derivatives designed as aromatase inhibitors were performed. As in previous studies for the validation of the molecular docking study with Glide SP, the cocrystal ligand ASD self-docking process was performed in the PDB ID: 3EQM structure selected for the aromatase enzyme [26]. The RMSD value of ASD between the docking pose and the natural bonding pose was measured as 0.0741 Å (Fig. 4A). A value of RMSD (Root Mean Square Deviation) below 3 Å may indicate that the accuracy of the docking pose is acceptable [27,28]. After the docking study was validated, Glide SP molecular docking was performed with active compounds **1a, 1b, 1d, 1k**, and letrozole, which is used as the standard drug in enzyme activity studies, with three-dimensional minimization structures created by OPLS4 field forces. As it is understood from molecular docking analysis, π-π stacking interactions with cofactor HEM in the enzyme structure are important for a compound to act as an aromatase inhibitor. In Fig. 4B, the binding pose and protein-ligand interactions of letrozole, and in Fig. 5, the binding poses of compounds **1a, 1b, 1d, and 1k** at the aromatase active site were given. In all 4 compounds, as in letrozole, it gives π-π stacking interactions with HEM and Trp224. Details of protein-ligand interaction patterns such as hydrogen bonding, positively charged, negatively charged, polar, and π-cation are given in Table 3. The compounds gave similar binding poses at the aromatase active site.

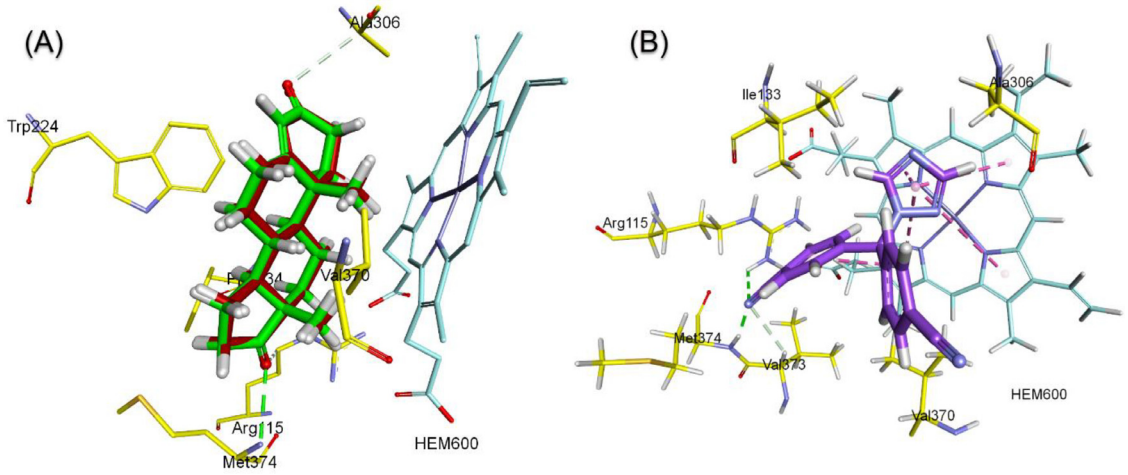

Fig. 4. (A) The natural binding pose (green) of cocrystal ASD in the aromatase enzyme structure and the binding pose of cocrystal ligand ASD obtained from Glide SP docking for the validation of molecular docking (orange) (RMSD: 0.0741 Å) (B) Binding pose of letrozole, an aromatase inhibitor, at the aromatase active site.

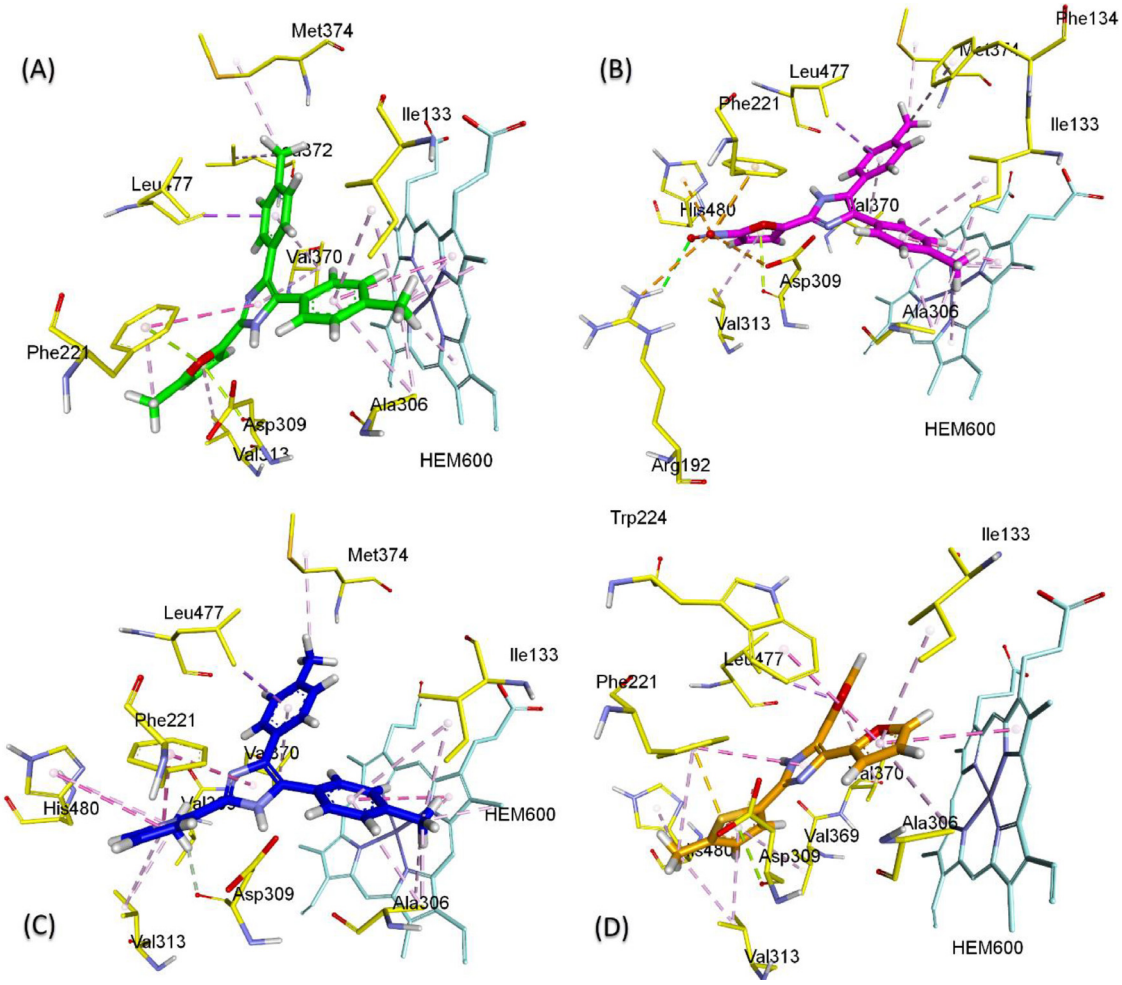

Fig. 5. Protein-ligand interactions derived from the Glide SP molecular docking study. The binding poses of (**A**) compound **1a**, (**B**) compound **1b**, (**C**) compound **1d,** and (**D**) compound **1k** at the active site of the human aromatase enzyme (PDB ID: 3EQM).

In addition, the protein-ligand interaction energies obtained from Glide SP ligand docking are shown in Table 3. In both cytotoxicity and aromatase enzyme *in vitro* experiments, the most active compound, **1a**, gave the highest interaction energy. Letrozole generated −6.876 kcal/mol binding energy, while the other compounds **1b, 1d**, and **1k** created interaction energies of −8.059 kcal/mol, −6.876 kcal/mol, and −6.054 kcal/mol, respectively. Other compounds **1c** (−7.565), **1d** (−6.876), **1e** (−7.466), **1f** (−7.707), 1 g (−7.133), 1 h (−6.124), **1i** (−5.967), **1j** (−6.621), **1k** (−6.054) and **1l** (−6.551) kcal/mol gave binding energy with the aromatase enzyme. Except for compounds **1a** and **1b**, there was no direct cor-

Table 3
Protein-ligand interaction energies (kcal/mol) in the aromatase active region of compounds **1a, 1b, 1d, 1k,** and letrozole and details of interaction types.

		Protein-ligand interactions	
Comp.	Glide Gscore	π-π stacking	Other types of interactions
1a	−8.224	Hem600 (5.30 Å), Trp224 (5.36 Å)	Arg115 and Arg192 (Positively Charged), Thr310, Hie480 and Ser478 (Polar) Glu302 and Asp309 Arg192 (Negatively Charged), Phe221, Ile305, Ala306, Val313, Val369, Val370, Leu372, Val373, Met373 and Leu477 (Hydrophobic)
1b	−8.059	Hem600 (5.30 Å), Trp224 (5.16 and 5.38 Å)	Arg192 (Salt Bridge, 4.44 Å), Hie480 (π-cation, 5.36 Å) and Phe221 (π-cation, 3.94 Å), Arg115 and Arg192 (Positively charged), Thr310, Hie480 and Ser478 (Polar) Glu302 and Asp309 (Negatively Charged), Ile133, Phe134, Phe221, Trp224, Ile305, Ala306, Val313, Val369, Val370, Leu372, Val373, Met374 and Leu477 (Hydrophobic)
1d	−6.876	Hem600 (5.38 Å), Phe221 (3.54 Å), Trp224 (5.17 Å)	Arg115 and Arg192 (Positively Charged), Thr310, Hie480 and Ser478 (Polar) Glu302 and Asp309 (Negatively Charged), Ile133, Phe134, Phe221, Ile305, Ala306, Val313, Val369, Val370, Leu372, Val373, Met374, Leu477, Leu477, leu479 (Hydrophobic)
1k	−6.054	Trp224 (5.37 Å)	Arg192 (Positively Charged), Thr310, Hie480 and Ser478 (Polar) Glu302 and Asp309 (Negatively Charged), Ile133, Phe134, Phe221, Trp224, Ile305, Ala306, Val313, Val369, Val370, Leu372, Val373, Leu477, leu479, Pro481 (Hydrophobic)
Letrozol	−6.876	Hem600 (4.09, 5.15 and 5.10 Å), Trp224 (5.47 Å)	Met374 (H bond, 1.81 Å), Arg115 (Positively Charged), Thr310 and Ser478 (Polar), Asp309 (Negatively Charged), Ile133, Phe134, Phe221, Trp224, Ile305, Ala306, Val313, Val369, Val370, Val373, Met374, Leu477 and Leu477 (Hydrophobic)

relation between Glide SP docking scores and aromatase enzyme inhibition.

2.6. ADME-Tox

Estimation of the absorption, distribution, metabolism, and excretion - toxicity (ADME-Tox) properties of newly synthesized compounds is useful to estimate some parameters computationally, given that many drug molecule candidates fail to reach their drug target due to poor ADME-Tox profile [29,30]. For this purpose, ADME-Tox estimates of active compounds **1a, 1b, 1d**, and **1k** were performed. The descriptor and druglikeness properties of the compounds were calculated with the SwissADME server. All the compounds shown in Table S1 do not deviate from Lipinski's five rules and Veber's rules. Compound **1a** shows one deviation from the limiting rules of Ghose, Egan, and Muegge as its hydrophobic character is higher than other compounds. The molecular weights of the compounds are below 500. Details of other descriptors LogP, rotatable bonds, acceptors, donors, and surface area are given in Table S1.

Computational ADME-Tox properties of compounds **1a, 1b, 1d**, and **1k** were determined via the pkCSM server. For absorption, the compounds showed low water solubility, Caco2 permeability was above the limit of 0.90, and the log Kp value found to be lower than −2.5, so it is skin permeable. Compounds other than **1k** showed no inhibition of P-glycoprotein. Distribution parameter, steady-state volume of distribution (VDss), log VDss ⟨ −0.15 and log VDss ⟩, since it was in the range of 0.45, thus, its low height is appropriate. Unbound rate to plasma proteins was low, except **1b** has BBB permeability, and all but **1k** have CNS permeability. It has the potential to exert inhibitory effects on many of the metabolic CYP enzymes. In excretion, the total clearance was lower than **1b**. Thus, It can be Organic Cation Transporter 2 (OCT2) substrate and interact with OCT2 inhibitors. In toxicity, however, compounds showed a positive AMES toxicity test, thus they may be mutagenic. Since the maximum tolerated doses were below 0.477 log (mg/kg/day), their tolerance is low. It is positive for hERG I and negative for hERG I, indicating the status of potassium channel blockers. Except for **1k**, the compounds showed no hepatotoxicity. There were no Skin Sensitizations. Since the toxicity value of *T. Pyriformis* protozoa bacteria was greater than −0.5 log ug/L, it has the potential to be toxic. Since IC_{50} values are not below 0.5 mM, Minnow fish did not show acute toxicity. More details of ADME-Tox profiles are given in Table S2.

3. Conclusion

In this study, 12 new imidazole derivative compounds were synthesized using the Debus-Radziszewski method. The structures of the original synthesized compounds were elucidated by ^{1}HNMR, ^{13}CNMR and Mass Spectroscopy method data.

When the cytotoxic effects of the synthesized compounds on the MCF7 cell line were evaluated, it was determined that the compounds **1a, 1b, 1d** and **1k** had promising effects in the series. In particular, the IC_{50} value (7.9 µM) of the compound **1a** was determined to be higher than cisplatin (9.75 µM). The L929 healthy mouse fibroblast cell line was used to determine the selectivities of the compounds. To identify the possible modes of action, aromatase inhibition experiments were performed for the most active compounds against the MCF-7 cell line. Further, the interactions between the best active compounds and the human aromatase cytochrome P450 (CYP) enzyme were analyzed through a molecular docking study. Finally, computational ADME-Tox studies of compounds **1a, 1b, 1d, and 1k** were performed and found to have the appropriate profile.

4. Experimental

All the chemicals employed in the synthetic procedure were purchased from Sigma-Aldrich Chemicals (Sigma-Aldrich Corp., St. Louis, MO, USA) or Merck Chemicals (Merck KGaA, Darmstadt, Germany). Melting points of the obtained compounds were determined by MP90 digital melting point apparatus (Mettler Toledo, OH, USA) and were uncorrected. ^{1}H NMR, and ^{13}C NMR spectra of the synthesized compounds were registered by a Bruker 500 MHz and 125 MHz digital FT-NMR spectrometer (Bruker Bioscience, Billerica, MA, USA) in DMSO–d6, respectively. Splitting patterns were designated as follows: s: singlet; d: doublet; t: triplet; m: multiplet in the NMR spectra. Coupling constants (J) were reported as Hertz. M+1 peaks were determined by Shimadzu LC/MS ITTOF system (Shimadzu, Tokyo, Japan). All reactions were monitored by thin-layer chromatography (TLC) using Silica Gel 60 F254 TLC plates (Merck KGaA, Darmstadt, Germany).

4.1. Chemistry

4.1.1. 4,5-Disubstituted-2-(5-substitutedfuran/thiophen-2-yl)−1H-imidazole (1a-11)

The mixture of benzyl derivative compound (0.02 mol), furan or thiophene aldehyde derivative compound (0.02 mol), ammonium acetate (0.12 mol) and 10 mL acetic acid was boiled under reflux for 3 h with stirring. The product was precipitated by pouring the mixture into ice water. The raw product was then washed with plenty of water and dried. The product was crystallized from aqueous ethanol.

4,5-Bis(4-methylphenyl)−2-(5-methylfuran-2-yl)−1*H*-imidazole (**1a**); Yield: 77%. M.p. 276.6 °C. ^{1}H NMR (300 MHz, DMSO–d_6): δ: 2.31 (6H, s, -CH_3), 2.37 (3H, s, -CH_3), 6.23–6.24 (1H, m, furan CH), 6.84–6.85 (1H, m, furan CH), 7.16 (4H, br.s., 1,4-disubstitutedbenzene), 7.37–7.39 (4H, m, 1,4-disubstitutedbenzene).^{13}C NMR (75 MHz, DMSO–d_6): δ: 13.86, 21.24, 21.50, 108.33, 108.66, 127.48, 127.87, 128.30, 129.40, 137.31, 138.99, 144.72, 152.28, 172.50. HRMS (*m/z*): $[M+H]^+$ calcd for $C_{22}H_{20}N_2O$ 329.1648; found:: 329.1638.

4,5-Bis(4-methylphenyl)−2-(5-nitrofuran-2-yl)−1*H*-imidazole (**1b**); Yield: 75%. M.p. 181.4 °C. ^{1}H NMR (300 MHz, DMSO–d_6): δ: 2.41 (6H, s, CH_3), 7.12–7.15 (1H, m, furan CH), 7.27–7.28 (1H, m, furan CH), 7.42 (4H, d, J = 6.06 Hz, 1,4-disubstitutedbenzene), 7.78–7.80 (4H, d, J = 6.12 Hz, 1,4-disubstitutedbenzene).^{13}C NMR (75 MHz, DMSO–d_6): δ: 21.50, 21.88, 110.66, 116.19, 127.60, 128.76, 129.37, 129.75, 130.08, 130.40, 130.50, 146.93, 172.48. HRMS (*m/z*): $[M+H]^+$ calcd for $C_{21}H_{17}N_3O_3$ 360.1343; found:360.1339.

4,5-Bis(4-methylphenyl)−2-(5-methylthiophen-2-yl)−1*H*-imidazole (**1c**); Yield: 77%. M.p. 107.5 °C. ^{1}H NMR (300 MHz, DMSO–d_6): δ: 2.30 (6H, s, -CH_3), 2.36 (3H, s, -CH_3), 7.13 (2H, d, J = 5.76 Hz, 1,4-disubstitutedbenzene), 7.27 (2H, d, J = 5.79 Hz, 1,4-disubstitutedbenzene), 7.38–7.45 (4H, m, 1,4-disubstitutedbenzene), 7.67–7.68 (1H, m, thiophene CH), 8.17–8.18 (1H, m, thiophene CH).^{13}C NMR (75 MHz, DMSO–d_6): δ: 13.54, 21.34, 21.51, 123.49, 124.94, 127.57, 128.66, 129.39, 129.84, 130.09, 130.51, 131.93, 139.41, 142.11. HRMS (*m/z*): $[M+H]^+$ calcd for $C_{22}H_{20}N_2S$ 345.1420; found: 345.1418.

4,5-Bis(4-methylphenyl)−2-(1-methyl-1*H*-pyrrol-2-yl)−1*H*-imidazole (**1d**): Yield: 79%. M.p. 118.3 °C. ^{1}H NMR (300 MHz, DMSO–d_6): δ: 2.37 (6H, s, CH_3), 3.87 (3H, s, CH_3), 6.22–6.23 (1H, m, pyrroleCH), 6.80–6.81 (1H, m, pyrrole CH), 6.97–6.99 (1H, m, pyrrole CH), 7.13 (2H, d, J = 6.63 Hz, 1,4-disubstitutedbenzene), 7.40–7.42 (4H, m, 1,4-disubstitutedbenzene), 7.86 (2H, d, J = 6.63 Hz, 1,4-disubstitutedbenzene).^{13}C NMR (75 MHz, DMSO–d_6): δ: 20.57, 21.51, 36.92, 108.30, 114.06, 114.53, 115.31, 125.87, 128.66, 130.01, 132.50, 138.61, 144.80, 152.17. HRMS (*m/z*): $[M+H]^+$ calcd for $C_{22}H_{21}N_3$ 328.1808; found: 328.1801.

4,5-Bis(4-fluorophenyl)−2-(5-methylfuran-2-yl)−1*H*-imidazole (**1e**): Yield: 75%. M.p. 255.3 °C. ^{1}H NMR (300 MHz, DMSO–d_6): δ: 2.38 (3H, s, CH_3), 6.25–6.26 (1H, m, furan CH), 6.84–6.85 (1H, m, furan CH), 7.14 (2H, br.s., 1,4-disubstitutedbenzene), 7.28 (2H, br.s., 1,4-disubstitutedbenzene), 7.47–7.52 (4H, m, 1,4-disubstitutedbenzene). ^{13}C NMR (75 MHz, DMSO–d_6): δ: 13.86, 108.40, 108.95, 116.26, 117.11, 129.44, 130.96, 133.43, 133.53, 139.26, 144.49, 152.50. HRMS (*m/z*): $[M+H]^+$ calcd for $C_{20}H_{14}N_2OF_2$: 337.1147; found: 337.1138.

4,5-Bis(4-fluorophenyl)−2-(5-nitrofuran-2-yl)−1*H*-imidazole (**1f**): Yield: 72%. M.p. 147.9 °C. ^{1}H NMR (300 MHz, DMSO–d_6): δ: 7.28 (1H, m, furan CH), 7.45–7.49 (4H, m, 1,4-disubstitutedbenzene), 7.52–7.56 (1H, m, furan CH), 8.02–8.06 (4H, m, 1,4-disubstitutedbenzene). ^{13}C NMR (75 MHz, DMSO–d_6): δ: 110.90, 116.10, 117.11, 117.34, 129.45, 129.47, 133.43, 133.53, 148.21, 165.45, 167.99. HRMS (*m/z*): $[M+H]^+$ calcd for $C_{19}H_{11}N_3O_3F_2$: 368.0841; found: 368.0835.

4,5-Bis(4-fluorophenyl)−2-(5-methylthiophen-2-yl)−1*H*-imidazole (1 g): Yield: 78%. M.p. 144.7 °C. ^{1}H NMR (300 MHz, DMSO–d_6): δ: 2.50 (3H, s, CH_3), 7.83–7.84 (1H, m, thiophene CH), 7.15 (2H, br.s., 1,4-disubstitutedbenzene), 7.30 (2H, br.s., 1,4-disubstitutedbenzene), 7.45–7.46 (1H, m, thiophene CH), 7.48–7.52 (4H, m, 1,4-disubstitutedbenzene). ^{13}C NMR (75 MHz, DMSO–d_6): δ: 21.50, 123.71, 124.75, 126.68, 127.80, 131.88, 133.79, 135.91, 138.31, 140.28, 142.17, 144.85. HRMS (*m/z*): $[M+H]^+$ calcd for $C_{20}H_{14}N_2F_2S$: 353.0919; found: 353.0903.

4,5-Bis(4-fluorophenyl)−2-(1-methyl-1*H*-pyrrol-2-yl)−1*H*-imidazole (1 h): Yield: 69%. M.p. 201.6 °C. ^{1}H NMR (300 MHz, DMSO–d_6): δ: 3.88 (3H, s, CH_3), 6.96–6.98 (1H, m, pyrrole CH), 7.13 (4H, d, J = 6.60 Hz, 1,4-disubstitutedbenzene), 7.25–7.26 (1H, m, pyrrole CH), 7.43–7.45 (1H, d, J = 6.42 Hz, pyrrole CH), 7.86 (4H, d, J = 6.57 Hz, 1,4-disubstitutedbenzene). ^{13}C NMR (75 MHz, DMSO–d_6): δ: 36.84, 114.34, 115.29, 124.29, 125.89, 126.58, 129.40, 132.31, 132.49, 139.81, 141.51, 158.80. HRMS (*m/z*): $[M+H]^+$ calcd for $C_{20}H_{15}N_3F_2$: 336.1307; found: 336.1300.

4,5-Di(furan-2-yl)−2-(5-methylfuran-2-yl)−1*H*-imidazole (**1i**): Yield: 78%. M.p. >350 °C. ^{1}H NMR (300 MHz, DMSO–d_6): δ: 2.34 (3H, s, CH_3),6.85–6.86 (2H, m, furan CH), 7.67–7.68 (2H, m, furan CH), 7.76–7.80 (1H, m, furan CH), 8.12–8.16 (1H, m, furan CH), 8.25 (2H, s, furan CH). ^{13}C NMR (75 MHz, DMSO–d_6): δ: 13.43, 107.60, 108.75, 114.05, 118.27, 120.04, 125.32, 126.71, 131.05, 131.55, 149.10, 151.39. HRMS (*m/z*): $[M+H]^+$ calcd for $C_{16}H_{12}N_2O_3$: 281.0921; found: 281.0910.

4,5-Di(furan-2-yl)−2-(5-nitrofuran-2-yl)−1*H*-imidazole (**1j**): Yield: 71%. M.p. >350 °C. ^{1}H NMR (300 MHz, DMSO–d_6): δ: 6.85–6.86 (2H, m, Furan CH), 7.40–7.41 (1H, m, Furan CH), 7.66–7.67 (2H, m, Furan CH), 7.85–7.86 (1H, m, Furan CH), 8.24–8.25 (2H, m, Furan CH). ^{13}C NMR (75 MHz, DMSO–d_6): δ: 109.67, 112.21, 114.06, 116.12, 125.33, 127.94, 129.09, 136.92, 139.38, 149.10, 151.40. HRMS (*m/z*): $[M+H]^+$ calcd for $C_{15}H_9N_3O_5$: 312.0615; found: 312.0610.

4,5-Di(furan-2-yl)−2-(5-methylthiophen-2-yl)−1*H*-imidazole (**1k**): Yield: 76%. M.p. >350 °C. ^{1}H NMR (300 MHz, DMSO–d_6): δ: 2.34 (3H, s, CH_3), 6.85–6.86 (2H, m, Furan CH), 7.67–7.68 (2H, m, Furan CH), 7.76–7.81 (1H, m, Furan CH), 8.12–8.16 (1H, m, Furan CH), 8.25 (2H, s, Furan CH). ^{13}C NMR (75 MHz, DMSO–d_6): δ: 21.57, 109.60, 112.13, 125.41, 125.69, 126.77, 128.23, 131.19, 139.15, 140.96, 142.44, 142.82. HRMS (*m/z*): $[M+H]^+$ calcd for $C_{16}H_{12}N_2O_2S$: 297.0692; found: 297.0684.

4,5-Di(furan-2-yl)−2-(1-methyl-1*H*-pyrrol-2-yl)−1*H*-imidazole (**1l**): Yield: 66%. M.p. 221.8 °C. ^{1}H NMR (300 MHz, DMSO–d_6): δ: 3.37 (3H, s, CH_3), 7.16–7.20 (2H, m, Aromatic CH), 7.32–7.36 (2H, m, Aromatic CH), 7.66–7.67 (2H, m, Aromatic CH), 8.03–8.06 (1H, m, Aromatic CH), 8.17–8.18 (2H, m, Aromatic CH). ^{13}C NMR (75 MHz, DMSO–d_6): δ: 36.20, 114.26, 114.75, 115.30, 123.24, 128.83, 130.19, 131.89, 132.49, 139.06, 142.30, 149.12. HRMS (*m/z*): $[M+H]^+$ calcd for $C_{16}H_{13}N_3O_2$: 280.1081; found: 280.1070.

4.2. Cytotoxicity assay

The anticancer activity of compounds **1a-1l** was screened according to the MTT assays. The MTT assays were performed as previously described [31]. Anticancer activity of final compounds was assessed against MCF-7 (human breast adenocarcinoma cell line) cell line as well as L929 (mouse fibroblast cell line). Cisplatin was used as the reference drug in the MTT assays.

4.3. Aromatase inhibition assay

This method was carried out according to the kit procedure (BioVision, Aromatase (CYP19A) Inhibitor Screening Kit (Fluorometric)).

4.4. Molecular docking

All stages of the molecular docking work were carried out with the Schrödinger Maestro version 2021.2. PDB ID:3EQM with a resolution of 2.90 Å was selected for the target cytochrome P450 CYP19A1 aromatase enzyme (https://www.rcsb.org/structure/3EQM) [32]. Protein preparation was done with the 'Protein Preparation Wizard' module. Water and other heteroatoms in the protein structure, except for the cofactor HEM (Iron-containing protoporphyrin IX), were removed and hydrogens were added. The assignment of the hydrogen bonds was optimized at PROPKA:7.0 using water molecule orientations. OPLS4 (Optimized Potential for Liquid Simulations) force fields were minimized by the aromatase enzyme. The compounds were drawn with ChemDraw Professional 17.0 and minimized using OPLS4 force fields at pH:7.2 with the 'LigPrep' module. Based on the cocrystal ligand ASD (4-androstene-3–17–dione), the active site coordinates were determined, and the grid file was created as 20×20×20 $Å^3$ with the 'Receptor Grid Generation' module. Ligand docking studies were performed with Glide Standard Precision (SP) [33]. Analysis and visualization of protein-ligand interactions were carried out with Maestro 'Ligand Interaction' module and BIOVIA Discovery Studio Visualizer v21.

4.5. ADME-Tox predictions

Computational estimation studies of absorption, distribution, metabolism, and excretion - toxicity (ADME-Tox) parameters of active molecules **1a, 1b, 1d** and **1k** were calculated using SwissADME (http://www.swissadme.ch/) and pkCSM server (http://biosig.unimelb.edu.au/pkcsm/) [34,35].

Declaration of Competing Interest

The authors declared no conflict of interest.

CRediT authorship contribution statement

Gökay Çetiner: Conceptualization, Visualization, Data curation, Formal analysis, Writing – review & editing. **Ulviye Acar Çevik:** Conceptualization, Visualization, Data curation, Formal analysis, Writing – review & editing. **Ismail Celik:** Conceptualization, Visualization, Data curation, Formal analysis, Writing – review & editing. **Hayrani Eren Bostancı:** Conceptualization, Visualization, Data curation, Formal analysis, Writing – review & editing. **Yusuf Özkay:** Conceptualization, Visualization, Writing – original draft, Writing – review & editing. **Zafer Asım Kaplancıklı:** Conceptualization, Visualization, Writing – original draft, Writing – review & editing.

Data Availability

Data will be made available on request.

Acknowledgments

The authors thank Ankara University-Scientific Research Unity for supplying the Schrödinger software purchased under grant project number BAP-21B0237004.

Supplementary materials

Supplementary material associated with this article can be found, in the online version, at doi:10.1016/j.molstruc.2023.134920.

References

[1] N.B. Sayyad, P.M. Sabale, M.D. Umare, K.K. Bajaj, Aromatase inhibitors: development and current perspectives, Indian J. Pharm. Educ. Res. 56 (2022) 311–320, doi:10.5530/ijper.56.2.51.

[2] H.R. Rashdan, I.A. Shehadi, Triazoles synthesis & applications as nonsteroidal aromatase inhibitors for hormone-dependent breast cancer treatment, Heteroatom Chem. (2022), doi:10.1155/2022/5349279.

[3] P.M. Sable, L.C. Potey, Synthesis and antiproliferative activity of imidazole and triazole derivatives of flavonoids, Pharma. Chem. J. 52 (2018) 438–443, doi:10.1007/s11094-018-1836-z.

[4] A.M. Prior, X. Yu, E.J. Park, T.P. Kondratyuk, Y. Lin, J.M. Pezzuto, D. Sun, Structure-activity relationships and docking studies of synthetic 2-arylindole derivatives determined with aromatase and quinone reductase 1, Bioorg. Med. Chem. Lett. 27 (2017) 5393–5399, doi:10.1016/j.bmcl.2017.11.010.

[5] M. Fantacuzzi, M. Gallorini, N. Gambacorta, A. Ammazzalorso, Z. Aturki, M. Balaha, … B. De Filippis, Design, synthesis and biological evaluation of aromatase inhibitors based on sulfonates and sulfonamides of resveratrol, Pharmaceuticals 14 (2021) 984, doi:10.3390/ph14100984.

[6] S. Begum, P. Jaswanthi, B.V. Lakshmi, K. Bharathi, QSAR studies on indole-azole analogues using DTC tools; imidazole ring is more favorable for aromatase inhibition, J. Indian Chem. Soc. 98 (2021) 100016, doi:10.1016/j.jics.2021.100016.

[7] S. Rani, K. Raheja, V. Luxami, K. Paul, A review on diverse heterocyclic compounds as the privileged scaffolds in non-steroidal aromatase inhibitors, Bioorg. Chem. 113 (2021) 105017, doi:10.1016/j.bioorg.2021.105017.

[8] S.P. Avvaru, M.N. Noolvi, T.M. Aminbhavi, S. Chkraborty, A. Dash, S.S. Shukla, Aromatase inhibitors evolution as potential class of drugs in the treatment of postmenopausal breast cancer women, Mini Rev. Med. Chem. 18 (2018) 609–621, doi:10.2174/1389557517666171101100902.

[9] K. Kaur, V. Jaitak, Recent development in indole derivatives as anticancer agents for breast cancer, Anti-Cancer Agents Med. Chem. 19 (2019) 962–983, doi:10.2174/1871520619666190312125602.

[10] A. Sood, D.K. Lang, R. Kaur, B. Saini, S. Arora, Relevance of aromatase inhibitors in breast cancer treatment, Curr. Top. Med. Chem. 21 (2021) 1319–1336, doi:10.2174/1568026621666210701143445.

[11] A. Ammazzalorso, M. Gallorini, M. Fantacuzzi, N. Gambacorta, B. De Filippis, L. Giampietro, … R. Amoroso, Design, synthesis and biological evaluation of imidazole and triazole-based carbamates as novel aromatase inhibitors, Eur. J. Med. Chem. 211 (2021) 113115, doi:10.1016/j.ejmech.2020.113115.

[12] J. Song, Z. Wu, B. Wangtrakuldee, S.R. Choi, Z. Zha, K. Ploessl, … H. Kung, 4-(((4-iodophenyl) methyl)-4H-1,2,4-triazol-4-ylamino)-benzonitrile: a potential imaging agent for aromatase, J. Med. Chem. 59 (2016) 9370–9380, doi:10.1021/acs.jmedchem.6b00849.

[13] R. Pingaew, P. Mandi, V. Prachayasittikul, S. Prachayasittikul, S. Ruchirawat, V. Prachayasittikul, Synthesis, molecular docking, and QSAR study of sulfonamide-based indoles as aromatase inhibitors, Eur. J. Med. Chem. 143 (2018) 1604–1615, doi:10.1016/j.ejmech.2017.10.057.

[14] F. Kalalinia, M. Jouya, A.K. Komachali, S.M. Aboutourabzadeh, G. Karimi, J. Behravan, … F. Hadizadeh, Design, synthesis, and biological evaluation of new azole derivatives as potent aromatase inhibitors with potential effects against breast cancer, Anti-Cancer Agents Med. Chem. 18 (2018) 1016–1024, doi:10.2174/1871520618666180116105858.

[15] K. Seth, S.K. Garg, R. Kumar, P. Purohit, V.S. Meena, R. Goyal, … A.K. Chakraborti, 2-(2-Arylphenyl) benzoxazole as a novel anti-inflammatory scaffold: synthesis and biological evaluation, ACS Med. Chem. Lett. 5 (2014) 512–516, doi:10.1021/ml400500e.

[16] S. Pancholia, T.M. Dhameliya, P. Shah, P.S. Jadhavar, J.P. Sridevi, P. Yogeshwari, … A.K. Chakraborti, Benzo[*d*]thiazol-2-yl (piperazin-1-yl) methanones as new anti-mycobacterial chemotypes: design, synthesis, biological evaluation and 3D-QSAR studies, Eur. J. Med. Chem. 116 (2016) 187–199, doi:10.1016/j.ejmech.2016.03.060.

[17] D. Kumar, D.N. Kommi, N. Bollineni, A.R. Patel, A.K. Chakraborti, Catalytic procedures for multicomponent synthesis of imidazoles: selectivity control during the competitive formation of tri-and tetrasubstituted imidazoles, Green Chem. 14 (2012) 2038–2049, doi:10.1039/C2GC35277J.

[18] D. Kumar, M. Sonawane, B. Pujala, V.K. Jain, S. Bhagat, A.K. Chakraborti, Supported protic acid-catalyzed synthesis of 2, 3-disubstituted thiazolidin-4-ones: enhancement of the catalytic potential of protic acid by adsorption on solid supports, Green Chem. 15 (2013) 2872–2884, doi:10.1039/C3GC41218K.

[19] D. Rajaraman, L.A. Anthony, P. Nethaji, R. Vallangi, One-pot synthesis, NMR, quantum chemical approach, molecular docking studies, drug-likeness and *in-silico* ADMET prediction of novel 1-(2, 3-dihydrobenzo [b][1, 4] dioxin-6-yl)-2-(furan-2-yl)-4, 5-diphenyl-1H-imidazole derivatives, J. Mol. Struct. 1273 (2023) 134314, doi:10.1016/j.molstruc.2022.134314.

[20] P.A. Nikitina, E.I. Basanova, E.B. Nikolaenkova, I.A. Os' kina, O.A. Serova, N.I. Bormotov, L.N. Shishkina, V.P. Perevalov, A.Y. Tikhonov, Synthesis of esters and amides of 2-aryl-1-hydroxy-4-methyl-1H-imidazole-5-carboxylic acids and study of their antiviral activity against orthopoxviruses, Bioorg. Med. Chem. Lett. 79 (2022) 129080, doi:10.1016/j.bmcl.2022.129080.

[21] U. Acar Çevik, B. Kaya Çavuşoğlu, B.N. Sağlık, D. Osmaniye, S. Levent, S. Ilgın, Y. Ozkay, Z.A. Kaplancıklı, Synthesis, docking studies and biological activity of new benzimidazole-triazolothiadiazine derivatives as aromatase inhibitor, Molecules 25 (2020) 1642, doi:10.3390/molecules25071642.

[22] N. Suvannang, C. Nantasenamat, C. Isarankura-Na-Ayudhya, V. Prachayasittikul, Molecular docking of aromatase inhibitors, Molecules 16 (2011) 3597–3617, doi:10.3390/molecules16053597.

[23] I. Celik, M. Erol, Z. Duzgun, In silico evaluation of potential inhibitory activity of remdesivir, favipiravir, ribavirin and galidesivir active forms on SARS-CoV-2 RNA polymerase, Mol. Divers (2021) 1–14, doi:10.1007/s11030-021-10215-5.

[24] I. Celik, T.E. Tallei, A computational comparative analysis of the binding mechanism of molnupiravir's active metabolite to RNA-dependent RNA polymerase

of wild-type and Delta subvariant AY. 4 of SARS-CoV-2, J. Cell. Biochem. 123 (2022) 807–818, doi:10.1002/jcb.30226.
[25] L. Giampietro, M. Gallorini, N. Gambacorta, A. Ammazzalorso, B. De Filippis, A.D. Valle, … R. Amoroso, Synthesis, structure-activity relationships and molecular docking studies of phenyldiazenyl sulfonamides as aromatase inhibitors, Eur. J. Med. Chem. 224 (2021) 113737, doi:10.1016/j.ejmech.2021.113737.
[26] U. Acar Çevik, I. Celik, A. Işık, I. Ahmad, H. Patel, Y. Özkay, Z.A. Kaplancıklı, Design, synthesis, molecular modeling, DFT, ADME and biological evaluation studies of some new 1, 3, 4-oxadiazole linked benzimidazoles as anticancer agents and aromatase inhibitors, J. Biomol. Struct. Dyn. (2022) 1–15, doi:10.1080/07391102.2022.2025906.
[27] İ. Çapan, A. Shehu, Y. Sert, İ. Çelik, M. Erol, İ. Koca, S. Servi, Synthesis, molecular docking, molecular dynamics and evaluation of Drug-Likeness properties of the fused N-Formyl pyrazoline substituted new dehydroepiandrosterone derivatives, J. Biomol. Struct. Dyn. (2022) 1–12, doi:10.1080/07391102.2022.2034667.
[28] U.A. Çevik, I. Celik, J. Mella, M. Mellado, Y. Özkay, Z.A. Kaplancıklı, Design, synthesis, and molecular modeling studies of a novel benzimidazole as an aromatase inhibitor, ACS Omega (2022), doi:10.1021/acsomega.2c01497.
[29] I. Celik, G. Ayhan-Kılcıgil, A. Karayel, B. Guven, A. Onay-Besikci, Synthesis, molecular docking, in silico ADME, and EGFR kinase inhibitor activity studies of some new benzimidazole derivatives bearing thiosemicarbazide, triazole, and thiadiazole, J. Heterocycl. Chem. 59 (2022) 371–387, doi:10.1002/jhet.4431.
[30] .... U.A. Çevik, I. Celik, A. Işık, R.R. Pillai, T.E. Tallei, R. Yadav, Z.A. Kaplancıklı, Synthesis, molecular modeling, quantum mechanical calculations and ADME estimation studies of benzimidazole-oxadiazole derivatives as potent antifungal agents, J. Mol. Struct. 1252 (2022) 132095, doi:10.1016/j.molstruc.2021.132095.
[31] U. Acar Çevik, B.N. Sağlık, D. Osmaniye, S. Levent, B. Kaya Çavuşoğlu, A.B. Karaduman, … Z.A. Kaplancıklı, Synthesis, anticancer evaluation and molecular docking studies of new benzimidazole-1, 3, 4-oxadiazole derivatives as human topoisomerase types I poison, J. Enzyme Inhib. Med. Chem. 35 (2020) 1657–1673, doi:10.1080/14756366.2020.1806831.
[32] D. Ghosh, J. Griswold, M. Erman, W. Pangborn, Structural basis for androgen specificity and oestrogen synthesis in human aromatase, Nature 457 (2009) 219–223, doi:10.1038/nature07614.
[33] R.A. Friesner, J.L. Banks, R.B. Murphy, T.A. Halgren, J.J. Klicic, D.T. Mainz, … P.S. Shenkin, Glide: a new approach for rapid, accurate docking and scoring. 1. Method and assessment of docking accuracy, J. Med. Chem. 47 (2004) 1739–1749, doi:10.1021/jm0306430.
[34] A. Daina, O. Michielin, V. Zoete, SwissADME: a free web tool to evaluate pharmacokinetics, drug-likeness and medicinal chemistry friendliness of small molecules, Sci. Rep. 7 (2017) 1–13, doi:10.1038/srep42717.
[35] D.E. Pires, T.L. Blundell, D.B. Ascher, pkCSM: predicting small-molecule pharmacokinetic and toxicity properties using graph-based signatures, J. Med. Chem. 58 (2015) 4066–4072, doi:10.1021/acs.jmedchem.5b00104.